Available online at www.sciencedirect.com
ScienceDirect
Polymer 48 (2007) 3213–3225
polymer
www.elsevier.com/locate/polymer

Nanoindentation of shape memory polymer networks

Edem Wornyo [a,*], Ken Gall [b,c], Fuzheng Yang [c], William King [c]

[a] School of Electrical and Computer Engineering, Georgia Institute of Technology, 777 Atlantic Drive, Atlanta, GA 30332, United States
[b] School of Materials Science and Engineering, Georgia Institute of Technology, Atlanta, GA 30332, United States
[c] Woodruff School of Mechanical Engineering, Georgia Institute of Technology, Atlanta, GA 30332, United States

Received 15 December 2006; received in revised form 6 March 2007; accepted 10 March 2007
Available online 14 March 2007

Abstract

This work examines the small-scale deformation and thermally induced recovery behavior of shape memory polymer networks as a function of crosslinking structure. Copolymer shape memory materials based on diethylene glycol dimethacrylate and polyethylene glycol dimethacrylate with a molecular weight of 550 crosslinkers and a *tert*-butyl acrylate linear chain monomer were synthesized with varying weight percentages of crosslinker from 0 to 100%. Dynamic mechanical analysis is used to acquire the bulk thermomechanical properties of the polymers, including the glass transition temperature and the elastic modulus over a wide temperature range. Instrumented nanoindentation is used to examine ambient temperature deformation of the polymer networks below their glass transition temperature. The glassy modulus of the networks measured using nanoindentation is relatively constant as a function of crosslinking density, and consistent with values extracted from monotonic tensile tests. The ambient temperature hardness of the networks increases with increasing crosslinking density, while the dissipated energy during indentation decreases with increasing crosslinking density. The changes in hardness correlated with the changes in glass transition but not changes in the rubbery modulus, both of which can scale with a change in crosslink density. Temperature induced shape recovery of the indentations is studied using atomic force microscopy. For impressions placed at ambient temperature, the indent shape recovery profile shifts to higher temperatures as crosslink density and glass transition temperature increase.

Keywords: Shape memory polymers; Nanoindentation; Crosslinking

1. Introduction

The convergence of micro-/nano-electromechanical systems (MEMS/NEMS) and biomedical industries is driving various material innovations, particularly in miniaturized polymer based devices [1]. Polymers are used extensively in the microelectronics industry [2], as sensing materials [3,4], lithography tools [5,6], and biomedical devices [7–16]. This onus on polymers requires that the materials possess different properties in order to reduce the cost of production, decrease the scale of devices, and offer devices with new functional properties. Many researchers have modified existing polymers by the addition or removal of tailored functional groups to make the polymers ''smart'', hence enhancing the material utility [17–25]. Shape memory polymers are a class of elastomer-like polymers that possess the ability to recover their original shape from a deformed shape upon the application of an external stimulus such as light, magnetic field, or heat [26–30].

A schematic representation of the shape memory effect in polymers is illustrated in Fig. 1. The shape memory effect may be demonstrated in an appropriate polymer by deforming the material in its polymerized form at a temperature, T_d, above the transition temperature, T_g; storage of the material in the pre-set form is accomplished by cooling to a temperature, T_s, below T_g. Recovery of the original shape is performed by heating the polymer to a temperature beyond T_g without constraint or under a constraining force, F_r [31]. In thermoplastics, the shape memory effect is dependent on the presence of a reversible soft phase with a low transition temperature and a hard phase with a high transition temperature in the polymer

* Corresponding author. Tel.: +1 4043850624; fax: +1 4048949140.
E-mail address: ejwornyo@ece.gatech.edu (E. Wornyo).

0032-3861/$ - see front matter © 2007 Elsevier Ltd. All rights reserved.
doi:10.1016/j.polymer.2007.03.029

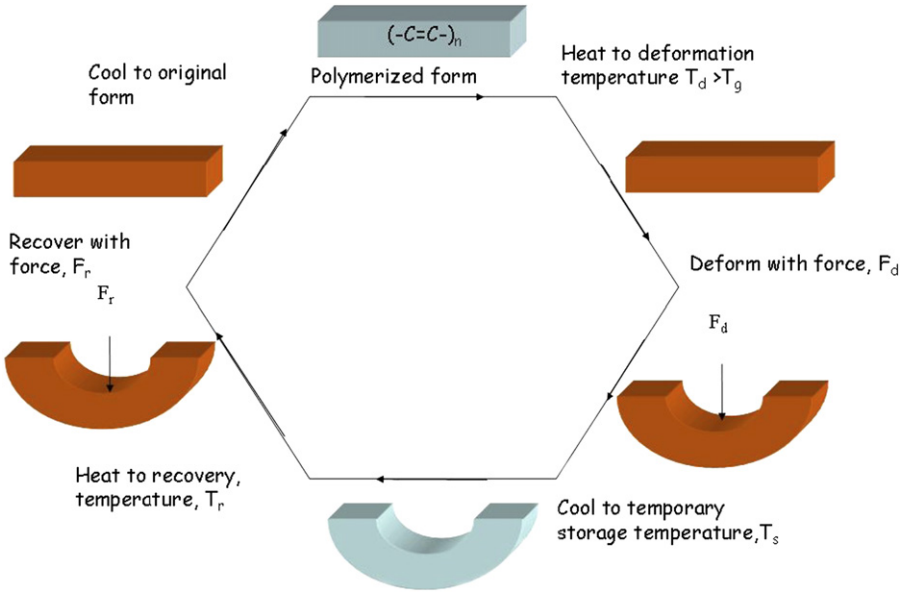

Fig. 1. Schematic of the shape memory principle.

mixture. The soft phase establishes the shape memory characteristics of the material while the hard phase provides physical crosslinking and determines the structural properties of the material. In thermoset polymers, chemical crosslinks facilitate shape memory and provide structural stability to the polymer at temperatures above the glass transition temperature in the rubbery plateau [32–34]. The shape memory effect in polymers is different from that of ceramics and metals due to the lower stresses and larger recoverable strains present in the polymers [35]. Although the shape memory effect is inherent to many chemically or physically crosslinked polymers, only polymers with elastomer type structures and tunable thermal transitions in the appropriate temperature range are useful shape memory polymers. In order to fully comprehend the suitability of shape memory polymers for various miniaturized biomedical and microsystems applications, it is necessary to characterize and understand their deformation and recovery response at sample surfaces and in small volumes of material.

Nanoindentation is a depth sensing technique used to probe the mechanical properties of nanometer scaled volumes of materials. This technique has been used extensively for the measurement of material properties of ceramics [36], biological specimens [37] and metallic alloys [38,39]. A full review of the use of nanoindentation in the aforementioned materials is beyond the scope of the present work, however, we will briefly discuss nanoindentation results on polymers. Nanoindentation has been employed by various groups to characterize the mechanical properties of a broad range of synthetic polymers. The majority of studies have focused on differences in indentation behavior of polymers with widely varying chemistries, or detailed analysis of the time-dependent viscoelastic behavior of polymers during indentation. The nanoindentation of polymers is particularly challenging due to their significant compliance and low hardness [40], viscoelastic or viscoplastic response [41], and resulting strain-rate dependence of deformation [42].

Despite these difficulties, researchers have made reasonable progress in the characterization of polymers using nanoindentation. Researchers have investigated the effects of indentation strain rate [42], backbone chemistry [43], processing technique [44,45], and annealing temperature [46]. Shen and coworkers [42] observed appreciable hardness dependence on strain rate for nylon 66 (PA66)/organoclay nanocomposites. Klapperich et al. [43] utilized nanoindentation to differentiate the nanomechanical properties of polymers of varying chemical structure. In an effort to determine the mechanical properties of polylactic acid (PLA), Wright-Charlesworth et al. utilized nanoindentation to determine the effect of processing methods and other factors on material characteristics [44]. Gregory and Spearing obtained increments in the modulus and hardness of in situ polymers compared to neat samples [45]. In a recent publication, Yu et al. [47] used nanoindentation to discover that the elastic modulus and hardness of the dielectric, hydrogen methyl silsesquioxane (HMSQ) matrix in a polyamidoamine (PAMAM) template decreased with increasing PAMAM concentration. Xu et al. recently used nanoindentation to measure the mechanical properties of a silicone elastomer. A decrease in hardness of the polymer was observed at an annealing temperature of 80 °C [46]. Juliano and coworkers [48] recently investigated structural properties of epoxy networks at room temperature, and at 55 °C. These researchers observed variations in creep compliance at 55 °C only. In addition, the researchers observed interplay between T_gs, molecular weight between crosslinks, and the creep compliance at 55 °C, but not at room temperature.

The shape memory effect in polymers has been almost exclusively investigated by macroscopic mechanical testing techniques. Notable among this is the work by Lee et al. [49] who investigated the effect of hard segment content on the shape memory properties of polyurethane (PU) using tensile testing. It was observed that the mechanical characteristics of the PU

were influenced by the degree of physical crosslinking in the material. Similarly, the work in Ref. [6] showed that mechanical properties of shape memory PUs can be enhanced via crosslinking. Tobushi et al. [50] investigated the shape fixity and shape recovery in polyurethane. The secondary-shape forming occurred only at a holding temperature above the glass transition temperature, and it was discovered that the rate of secondary-shape forming was directly proportional to the T_g. In related work, Park and coworkers [51] considered the effect of different crosslinking methods on the elastic modulus of ultra-high-molecular-weight polyethylene (UHMWPE). The investigation concluded that the crosslinking process determines the change in the elastic modulus when the crosslinked polymer is subjected to uniaxial tension. Upon subjecting the polymers to thermomechanical forces, it was discovered that the change in the storage moduli and the loss moduli also depend on the crosslinking method.

Very few researchers have investigated the shape memory properties of polymers at the submicron scale in chemically crosslinked polymer networks. Nelson and coworkers [52] examined the shape recovery of AFM indents in a thermoset polymer; they found the recovery to be dependent on temperature with full recovery at a temperature in close proximity to the glass transition temperature. Gall and coworkers [31] utilized microindentation to study the recovery of indents in a two-part epoxy shape memory polymer for microfluidic applications; these researchers observed 100% recovery of the indents. However, prior work has not examined the effect of variation in crosslink density on the mechanical properties of shape memory polymers using nanometer scale probe techniques.

The objective of the present study is to understand the effect of polymer structure on the formation and recovery of nanometer scale indents in shape memory polymer networks. Emphasis is placed on studying the dependence of indentation response on both glass transition temperature and rubbery modulus, through changes in crosslinking density and crosslinker molecular weight. We determine baseline polymer properties using bulk dynamic mechanical analysis and tensile testing. Small-scale deformation and recovery properties in the polymers are measured using nanoindentation and atomic force microscopy, respectively. Careful attention is given to the importance of area function in the extraction of quantitative properties from the nanoindentation curves. The results provide a framework for the comprehension of crosslinking effects on the nanoscale recovery response of shape memory polymer networks.

2. Analysis tools

Here we briefly review the relevant tools for analysis of nanoindentation data. It is important to note that the tools presented here have been developed be prior authors and [53,40] and we only summarize them here to provide guidance for fully understanding our results. We mention upfront that elasto-plastic tools are used to analyze the deformation behavior of the indents in the polymer networks. Although the networks clearly demonstrate viscoelasticity in the vicinity of their glass transition temperature, all indentations were performed in the polymers' glassy state at ambient temperature. In the glassy state, elasto-plastic behavior is a reasonable assumption regarding the polymer's response to small deformations during unloading. Although some time-dependent effects will be observed during unloading of the polymers in its glassy regime (rooted in the rate-dependent processes occurring during the large strain plastic deformation during the indentation, which induces local conformational changes in the polymer), these effects can be dealt with in accordance with similar effects observed during the nanoindentation of metals at room temperature (e.g. allowing relaxation through a hold prior to unloading). Temperature induced recovery behavior of the indents is time-dependent by nature, and the analysis tools used in this section were not used during interpretation of atomic force microscope based recovery experiments when the material transitions into a viscoelastic state.

A schematic of a representative nanoindentation experiment is shown in Fig. 2, with the pertinent features labeled. In Fig. 2b, the material surface is penetrated with an indenter tip of load P_{max} leading to a penetration depth, h, of the tip into the surface. The instrument continuously monitors the load and the corresponding depth with time. The resulting load-displacement curve is illustrated in Fig. 2a.

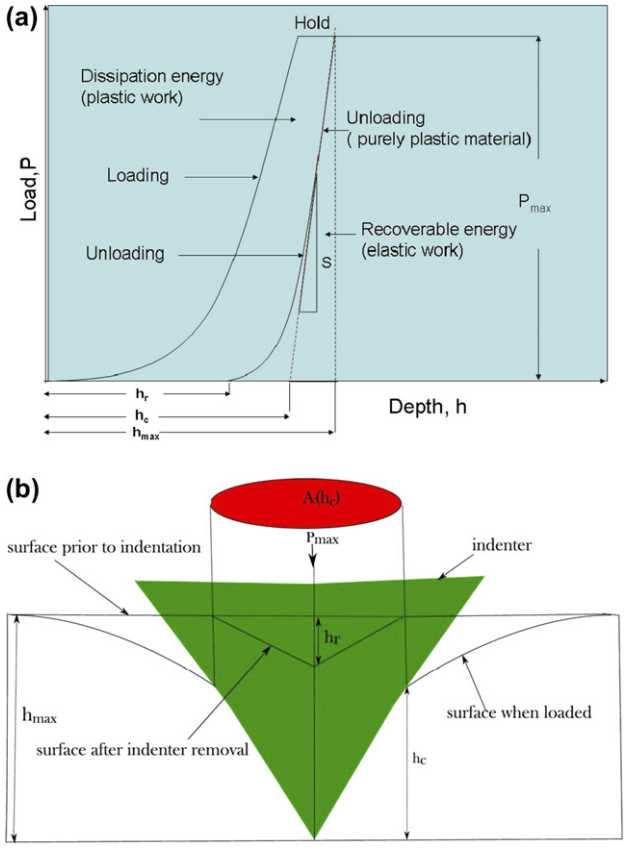

Fig. 2. Diagrammatic representation of the load–depth curve from a typical nanoindentation experiment. Here, h_r denotes the residual depth, h_c is the contact depth, h_{max} is the maximum depth reached by the indenter tip at maximum force of P_{max}.

Indentation hardness is defined as applied load per unit area of indentation. For a maximum load of P_{max} and a projected contact area of $A(h_c)$, as a function of the contact depth, h_c, the indentation hardness is defined as:

$$H = \frac{P_{max}}{A(h_c)} \tag{1}$$

The nanoindentation parameters may be extracted via the Oliver–Pharr model [53] from an experimental plot similar to Fig. 2a. The gradient of the initial portion of the unloading stiffness curve provides the elastic parameters of the material given that creep effects are dissipated through a hold and the material is not in the regime relative to T_g where viscoelasticity is dominant [40,53]. The gradient, or unloading stiffness, S is given by

$$S = \frac{dP}{dh} \tag{2}$$

A central challenge in interpreting indentation results is the determination of the contact area, $A(h_c)$. According to Oliver and Pharr [53], the determination of $A(h_c)$ may be done by estimating the contact depth, h_c, from the equation:

$$h_c = h_{max} - \varepsilon\frac{P_{max}}{S} \tag{3}$$

for a geometrical constant ε. The effective (reduced) elastic modulus, E_r, is expressed as

$$\frac{1}{E_r} = \frac{\left(1-\nu_m^2\right)}{E_m} + \frac{\left(1-\nu_i^2\right)}{E_i} \tag{4}$$

where E and ν are the elastic modulus and the Poisson's ratio, respectively, and the subscripts m and i refer to the material and the indenter, respectively. The relationship between the stiffness, S, and the reduced modulus is

$$S = 2aE_r = \frac{2\beta E_r\sqrt{A}}{\sqrt{\pi}} \tag{5}$$

where β is a constant. For a perfect Berkovich tip, the area function may be represented by $A = 24.5h_c^2$. For an indenter with a tip imperfection, the area may be described by

$$A(h_c) = 24.5h_c^2 + \sum_{i=0}^{7} a_i h_c^{\frac{1}{2^i}} \tag{6}$$

The a_is are coefficients which are typically determined by performing indents of varying depths in a material of known modulus. The indenter tip calibration is a critical step in interpretation since manufacturer's specification is often inaccurate and chemical and mechanical imperfections will invariably exist on the tip [41]. The material commonly used as a standard is fused silica (quartz) since its elastic modulus does not vary appreciably with depth and it does not contain a surface "layer" such as a surface oxide in metals. However, previous researchers have demonstrated [43] that it is necessary to use a standard material with a modulus in the vicinity of that of the sample being investigated to gain accuracy at relevant indentation depths. Fig. 5 shows a comparison of the area function of the Berkovich tip for PC, PMMA and quartz. The PC standard was used to calculate area function for the analysis presented in this work. Use of quartz as a standard did not change the trend effects observed here; however, the magnitude of the polymer's elastic modulus was unreasonable. This error comes from the fact that the fit to quartz is accurate at low loads (where it was fit), and very large loads, where the tip shape function does not matter, but inaccurate at intermediate loads.

3. Experimental method

Shape memory polymers based on a diethylene glycol dimethacrylate (DEGDMA) crosslinker, a polyethylene glycol dimethacrylate (PEGDMA) crosslinker with a molecular weight of 550, a *tert*-butyl acrylate (*t*BA) monomer, and the photoinitiator, 2,2-dimethoxy-2-phenyl acetophenone (DMPA) were designed. All chemicals were used as received (Sigma–Aldrich, St. Louis, MO). Weight percentages of the crosslinker and monomer from 0 to 100 were prepared with 1 wt% photoinitiator added to each mixture in glass vials. A magnetic stirrer was used to mix the mixtures thoroughly. Table 1 depicts the nomenclature of material mixtures used in the present experiment. Microscope glass slides, coated with Rain-X, were made into molds of dimensions 75 mm × 25 mm × 1 mm and 75 mm × 75 mm × 1 mm for dynamic mechanical analysis (DMA) and tensile testing samples; similar molds were made with a spacer of 300 μm for atomic force microscopy (AFM) and nanoindentation experiments. The mixtures were pipetted into the molds and ultraviolet (UV) polymerized (B100AP Blak Ray, UVP, Upland, CA) at an intensity of 10 mW/cm^2 for 10 min. In order to determine the thermomechanical

Table 1
Nomenclature and crosslink density/spacing for all materials in the present experiment are displayed here

Material name	Concentration of constituents (wt%)			E_r (GPa) at 448 K	Crosslink	
	DEGDMA	PEGDMA550	*t*BA		Density (nm^{-3})	Spacing (nm)
100*t*BA	0	0	100	NA	NA	NA
10DEG90*t*BA	10	0	90	2.5	0.135	1.95
20DEG80*t*BA	20	0	80	6	0.323	1.46
50DEG50*t*BA	50	0	50	14	0.755	1.09
100DEG	100	0	0	NA	9.63[a]	0.47
25DEG25PEG50*t*BA	25	25	50	11.5	0.620	1.17

[a] Estimated from a molecular size of 4.7 Å (Ref. [54]).

properties of these polymers, samples of dimension 25 mm × 4 mm × 1 mm were cut for DMA using a laser cutter. TA Instruments DMA Q 800 (TA Instruments Inc., Newcastle, DE) was used to obtain the dynamic mechanical properties of the copolymers in tensile mode. Heating and cooling rates of 3 °C/min, and a sampling rate of 1 Hz were used for all DMA tests. To obtain information on the variation of the glass transition temperature, five independent DMA runs were performed and the average and standard deviations were calculated. Table 2 displays information on the number of data points used to calculate the statistical distribution.

Four samples of dimensions ~3 mm × 3 mm were cut out from the center of the samples and affixed to atomic force microscopy (AFM) discs with superglue. The average surface roughness at room temperature of the samples polymerized against a glass slide was 7 ± 3 nm, as measured with the AFM in contact mode. Quasi-static nanoindentation was carried out on the samples using a nanoindenter (Triboscope, Hysitron Inc., Minneapolis, MN) with a Berkovich tip (a three-sided pyramidal diamond tip). The instrument is enclosed in an environmental isolation chamber to reduce external interferences. A peak load of 5 mN with a loading/unloading rate of 500 μN/s, and a hold time of 2 s at the maximum load was used. A maximum drift rate of 20 nm/s was set for the experiment. Four 3 × 3 arrays of indents were performed on each material sample. The indentations were performed in the central regions of the polymer samples to eliminate edge effects. Load–depth curves were analyzed for each of the 36 indents using the Oliver–Pharr model [53] to determine the reduced modulus (E_r) and the hardness (H) of the DEGDMA-*co*-*t*BA samples. E_r was extracted from 20% to 95% of the incipient unloading curve, while H was derived from Eqs. (1)–(3). Further, the results from the four 3 × 3 arrays were averaged, and the mean and standard deviation found for each wt% crosslinker (refer to Table 2 for total number of points). The dissipation energy was calculated from the area enclosed by the loading and unloading curves for each wt% crosslinker using MATLAB®.

Standard ASTM samples were laser-cut for tensile testing. The edges of the laser-cut samples were trimmed with sandpaper. The samples were then tested with a 2 kN load cell using an MTS Insight 2 (MTS Systems, Eden Prairie, MN) tensile tester at an applied displacement rate of 3 mm/s. An average of five results for each crosslinker concentration was taken.

The indented samples were transferred to the AFM (Asylum Research, Santa Barbara, CA) for the measurement of indent profile during temperature induced recovery. The indents were first located and imaged, and a scan of the surface profile was then performed as a function of increasing temperature at a rate of 1 °C/min from room temperature to a temperature above T_g of the material until the indents were fully recovered. A scan rate of 2 Hz or 1 min/frame was used in the AFM recovery experiments. Tuning of the cantilever was performed to minimize temperature effects on imaging. The topography of indents at each temperature was analyzed with the Asylum Research software. The difference in height between the highest crest and the lowest trough was recorded as the peak-to-peak height of the indents.

Table 2
Information on the number of duplicate samples and total number of data points used to determine the statistical distribution in this paper

Analysis technique	Number of duplicate samples	Number of tests performed on each sample	Total number of data points
Dynamic mechanical analysis	5	1	5
Nanoindentation	4	9	36

Total number of data points for dynamic mechanical analysis and nanoindentation were 5 and 36, respectively.

4. Results and discussion

Experimental results from measurements made in the present work are presented in Figs. 3–8. Dynamic mechanical analysis (DMA) thermograms measured for the DEGDMA-*co*-*t*BA samples in tensile mode is shown in Fig. 3a. The figure demonstrates that the glass transition temperature, T_g, and rubbery modulus, E_r, of the material vary appreciably with crosslinker percentage, while the glassy modulus remains relatively constant within experimental error (more detailed glassy modulus data to be shown in latter graphs). The storage modulus in Fig. 3a is approximately 3 GPa at temperatures less than T_g and then proceeds through a transition to the rubbery regime above T_g. A controlled variation in T_g and E_r is fundamental to the use of a polymer network in shape memory applications. It is evident from Fig. 3a that a rubbery plateau is absent for the thermoplastic material, 100*t*BA, as it has no chemical or significant physical crosslinks. Instead of a rubbery plateau, the material flows after going through the glass transition, characteristic of a single-phase amorphous thermoplastic. It is also observed in Fig. 3a that there is no transition to a rubbery state for 100DEG. The lack of glass transition for the highly crosslinked 100DEG is due to the significant density of crosslinking imparted by the short di-functional DEGDMA molecules, as evident in Table 1. Such a heavily crosslinked network is relatively immobile at all temperatures since chemical netpoints are in close vicinity. In between these extremes, the addition of the di-functional crosslinking agent to the linear *t*BA material results in a systematic increase in the glass transition temperature. For the short DEGDMA crosslinker, the increase in T_g comes principally from the local restriction to coordinated conformational motions at network points. As the density of network points increases, the effective volume of material restricted from coordinated conformational motion increases, and the material gradually loses the ability to create appreciable free volume with a temperature change, and its glass transition disappears. It is important to note that T_g of all polymers (those with a definable T_g) is above ambient temperature (25 °C) as illustrated in Fig. 3c.

In addition to a shift in the glass transition temperature, increased DEGDMA crosslinker concentration results in an increase in the rubbery modulus plateau (Fig. 3a). The increase in rubbery modulus is driven by an average shortening of the elastically active chain length between chemical netpoints.

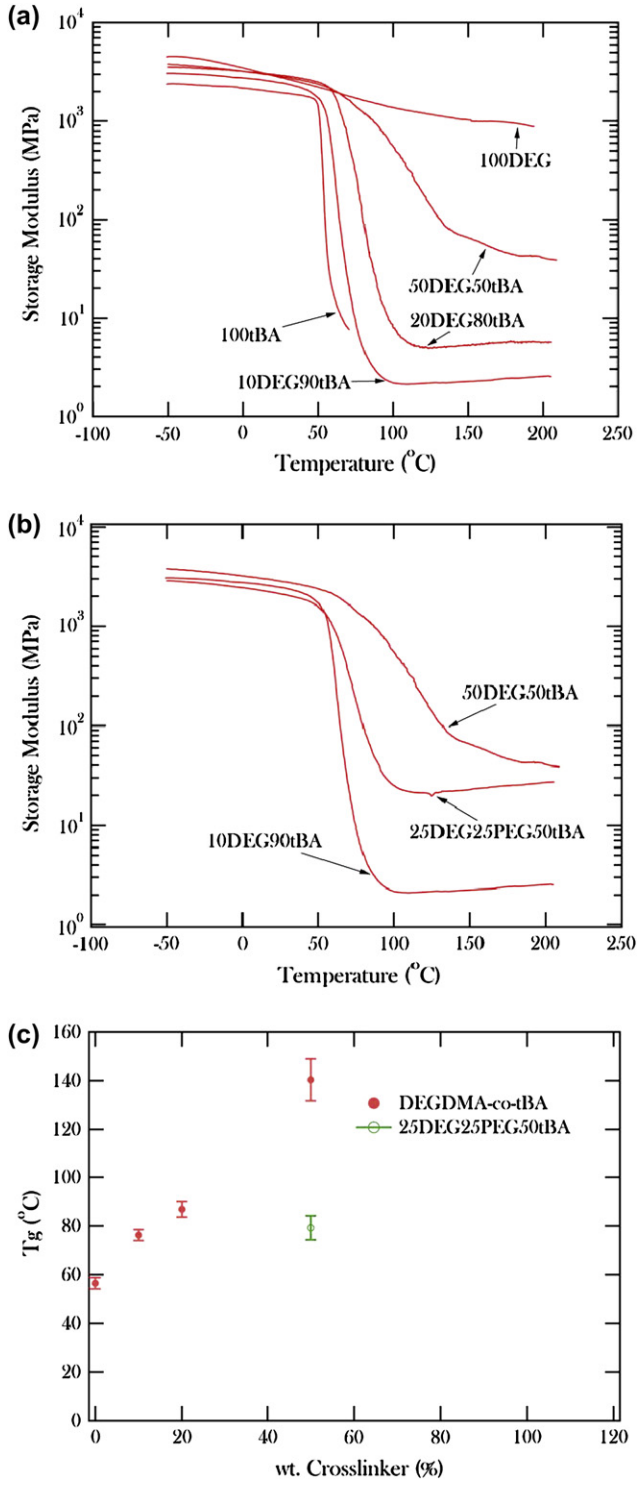

Fig. 3. (a) Thermomechanical properties of the DEGDMA-*co*-*t*BA shape memory polymers with respect to weight percent. The plot shows a gradual variation in the glass transition temperature and the storage modulus as the weight percent of the constituents of the polymer is varied. (b) Comparison of the thermomechanical characteristics of 10DEG90*t*BA, 50DEG50*t*BA and 25DEG25PEG50*t*BA. It is realized that 10DEG90*t*BA and 25DEG25-PEG50*t*BA have similar T_gs, and the rubbery modulus of 25DEG25PEG50*t*BA and 50DEG50*t*BA are in close proximity. (c) A synopsis of the glass transition temperatures of materials here. It is seen in this plot that the glass transition temperature increases with increasing crosslinker for the DEGDMA-*co*-*t*BA system. Since the glass transition temperature is based on a transition from the glassy state to the rubbery state, there is no T_g for the 100DEG which has no transition due to its small distance between crosslinks. The figure also displays the T_g of 25DEG25PEG50*t*BA.

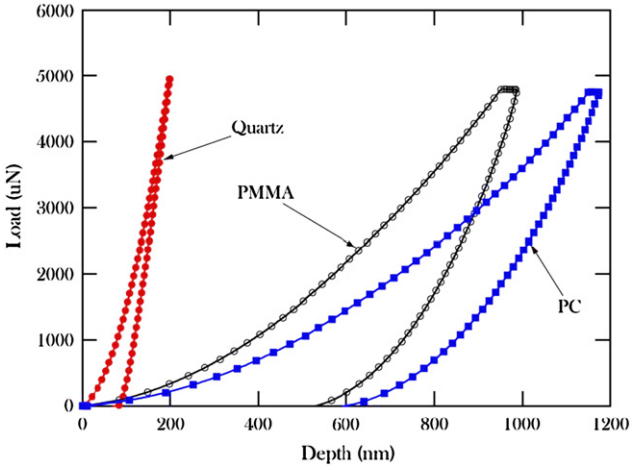

Fig. 4. Standard materials used for calculating the area function of the Berkovich tip. Polycarbonate (PC) has a modulus in the vicinity of that of the DEGDMA-*co*-*t*BA polymers and was chosen as the standard for the calculation.

From the theory of rubbery elasticity, $E_r = 3kT\nu_e$ where k is the Boltzmann's constant, T is the temperature corresponding to the DMA rubbery modulus, and ν_e is the crosslink density. Table 1 is a compilation of ν_e for the various wt% crosslinkers used in the present study. The table also includes a calculation of the crosslink spacing between molecules for all materials with a definable rubbery modulus, based on the premise of uniform crosslink distribution. According to Ref. [54], estimation of crosslink parameters from the rubbery modulus of highly crosslinked materials is not recommended. It should be noted here that the crosslink spacing and density for 100DEG was estimated from a molecular size of 4.7 Å, as reported in Ref. [54]. It is evident from the table that the crosslink spacing decreases with an increase in wt% crosslinker, as expected for the DEGDMA-*co*-*t*BA series of materials.

The results in Fig. 3a represent the influence of increasing crosslinking in *t*BA without a significant copolymer effect, due to the short length of the DEGDMA crosslinking molecules. The pure crosslinking effect leads to both an increase in glass transition temperature and rubbery modulus with increasing crosslinker addition. It is possible to counterbalance the crosslinking effect with a copolymer effect by lengthening the crosslinker through the use of PEGDMA 550. By replacing a fraction of the DEGDMA, with PEGDMA, the rubbery modulus will remain relatively constant, while the T_g will decrease relative to use of pure DEGDMA due to the lower glass transition temperature of PEGDMA. The aforementioned effect allows one to separate the effects of glass transition and rubbery modulus on nanomechanical properties, since these two effects are convoluted in the materials in Fig. 3a. In Fig. 3b we present a representative storage modulus curve for a new material, 25DEG25PEG50*t*BA, where 25% of the DEGDMA has been replaced by 25% PEGDMA. This new material has a glass

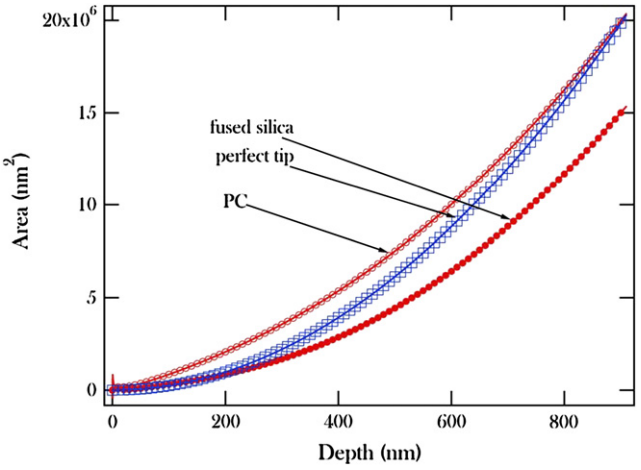

Fig. 5. Plots of calculated area functions based on the assumption of a perfect Berkovich tip, quartz and PC. The area function is pivotal in the determination of material properties such as elastic modulus and hardness.

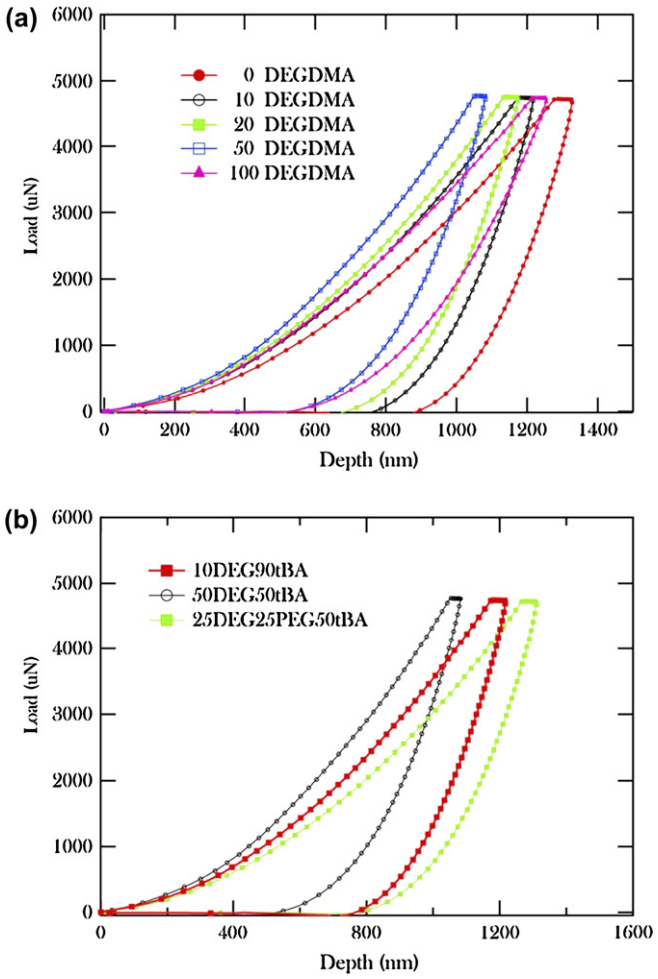

Fig. 6. (a) Representative load–depth plots of indentations at a maximum load of 5 mN on the DEGDMA-*co*-*t*BA samples. (b) Juxtaposition of the nanoindentation curves of 10DEG90*t*BA, 50DEG50*t*BA and 25DEG25PEG50*t*BA.

transition onset similar to the 10DEG90*t*BA material (see Fig. 3c for averaged T_g data), but a rubbery modulus plateau approaching the 50DEG50*t*BA material. Comparison amongst

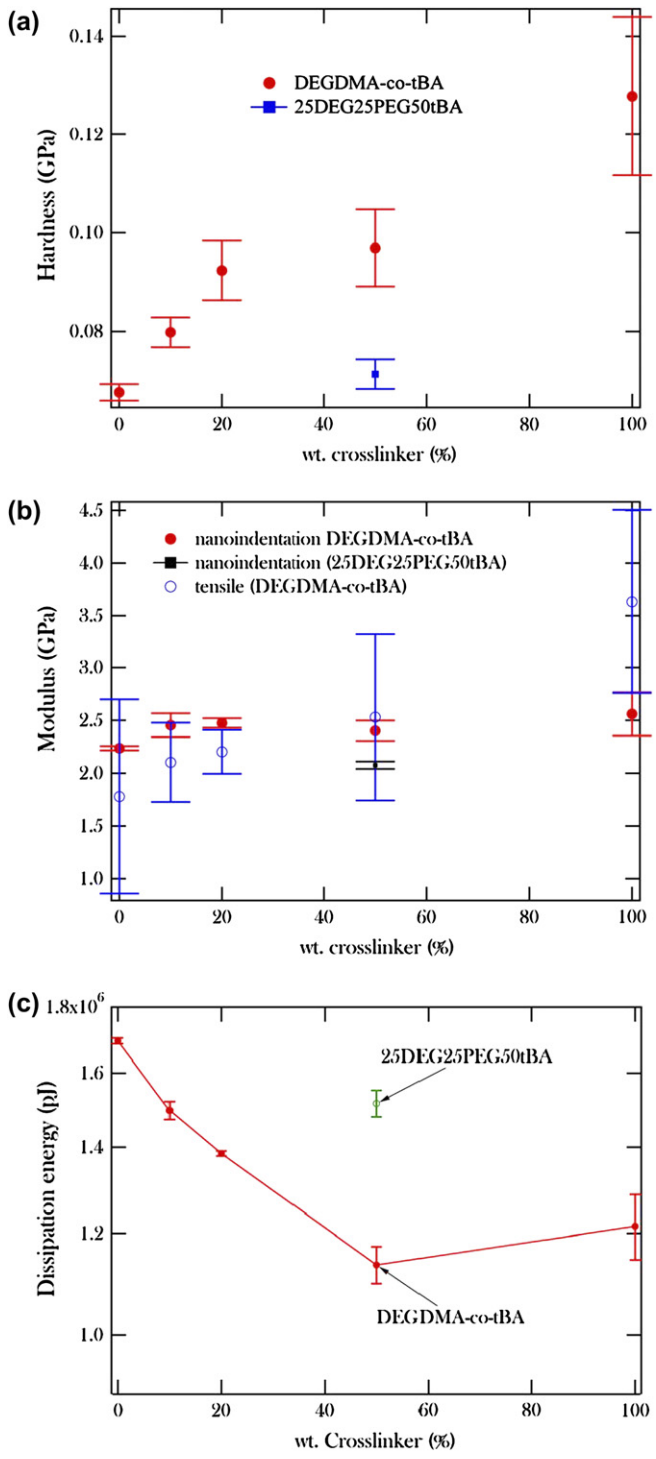

Fig. 7. (a) Hardness as a function of weight percent crosslinker within one standard deviation from the mean. All data points represent 36 measurements on various duplicate samples. The weight percent crosslinker represents the total amount of crosslinker (DEGDMA plus PEGDMA where appropriate). (b) Statistical distribution of the nanoindentation and tensile modulus as a function of the weight percent of DEGDMA crosslinker within one standard deviation from the mean. The weight percent crosslinker represents the total amount of crosslinker (DEGDMA plus PEGDMA where appropriate). (c) Dissipation energy as a function of crosslink density. The error bars are within a standard deviation from the mean. The weight percent crosslinker represents the total amount of crosslinker (DEGDMA plus PEGDMA where appropriate).

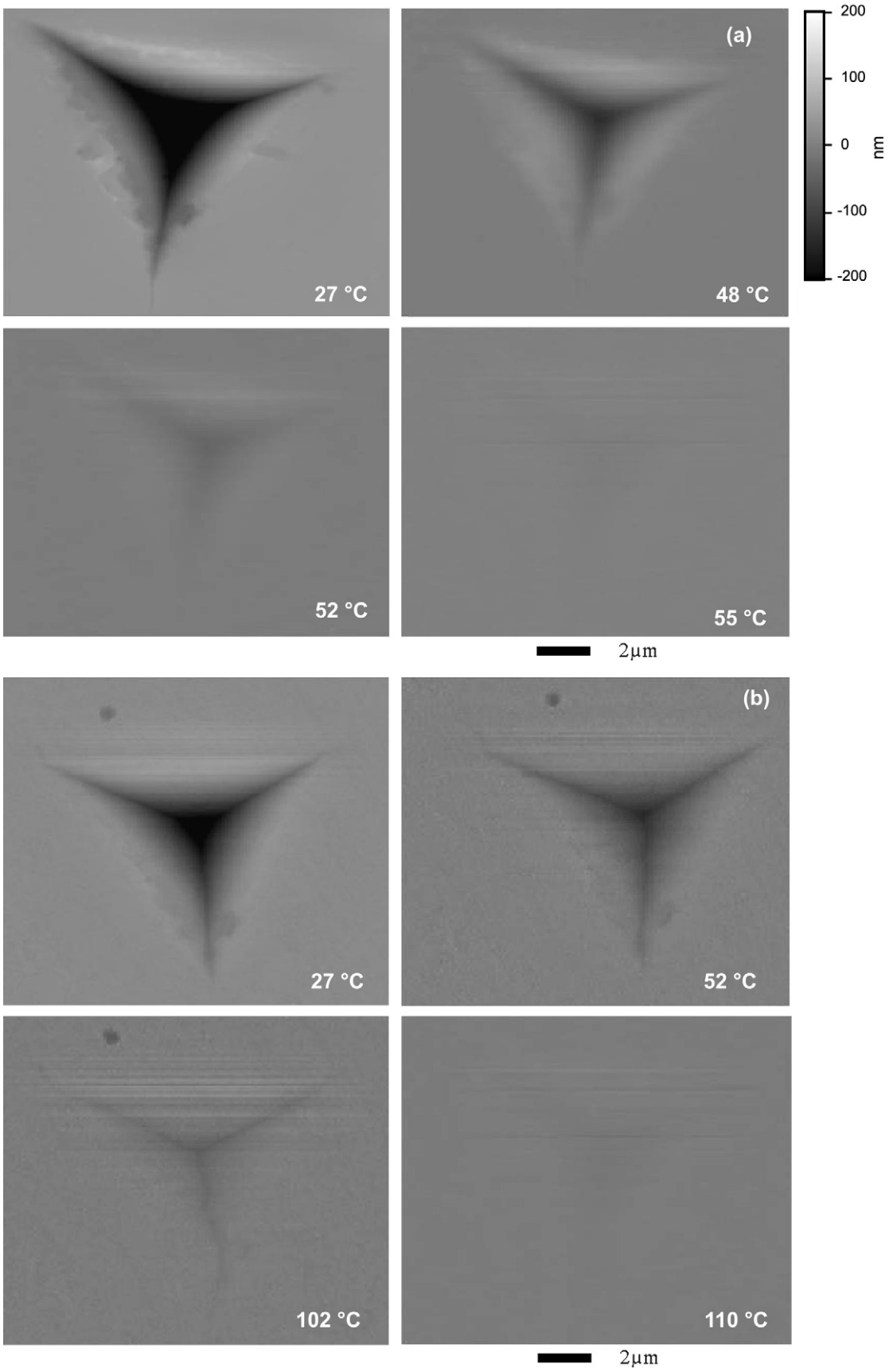

Fig. 8. Tapping mode AFM images showing evolution of shape recovery from room temperature to the recovery temperature for (a) l00*t*BA, and (b) 50DEG50*t*BA. It is noted that the indents shrink as temperature is increased. The indents eventually diminish in the vicinity of T_g for each material.

these three materials allows evaluation of the relative role of T_g versus E_r during interpretation of nanoindentation results.

In nanoindentation, an accurate extraction of the area function is central to the determining nanoscale material parameters such as hardness and reduced modulus. As a result, the selection of a standard material for the calibration of the indenter tip is paramount [43]. The use of the fused silica (quartz) calibration standard, often used for hard materials, has been shown to provide inadequate results for polymers [55]. The researchers in Ref. [43] proposed the use of a standard with properties close to that of the materials under study, hence our choice of PC whose properties are in the vicinity of the polymers used here. Fig. 4 displays load–depth curves of the standard materials considered in this research. Generally, the steeper the slope of the unloading portions of an indentation curve, the stiffer the material. Material hardness can be inferred from the load–depth curve through a steeper loading curve and a small residual depth at the point of unloading. It is seen from this figure that quartz is the stiffest, whereas PMMA and PC have similar stiffness. PC was chosen over PMMA as the nanoindentation data of PC does not change appreciably with loading rate at room temperature [43]. Moreover, PC's hardness and modulus are within the vicinity of the polymer networks used in this investigation, which are slightly softer than PMMA. Fig. 5 displays the area function for a perfect uncompensated Berkovich tip, along with area functions based on elastic modulus fits to quartz and PC standards. In particular, these results illustrate the possible margins of error which may be incurred as a result of assuming a perfect tip, and choosing a standard calibration material with nanomechanical properties different from the materials under study.

Berkovich indentation load–depth curves representing various wt% DEGDMA-*co*-*t*BA samples at a maximum load of 5 mN are presented in Fig. 6a. Results from studies at different indentation depths and loads will be presented in future work. Based on analysis of multiple load–depth curves, the nanomechanical properties of the networks demonstrate a statistically significant dependence on crosslink density at ambient temperature. At elevated temperatures, the networks would possess an even more significant difference in nanomechanical properties due to their differences in glass transition temperatures, an effect that is sometimes overlooked in indentation studies on various polymers. In Fig. 6b, we compare the load–depth curves of 10DEG90*t*BA, 50DEG50*t*BA, and 25DEG25PEG50*t*BA. There is also a difference in the nanomechanical properties of the materials in Fig. 6b, which have controlled differences in E_r and T_g. From the data in Fig. 6a, one would generally conclude that the materials become harder at ambient temperature (load–depth curves shift left and/or intersect at shallower depths at zero load) as crosslinking density is increased. However, relating this increase to fundamental properties of the polymer networks (E_r and T_g) is difficult since both E_r and T_g increase with increasing DEGDMA crosslinker concentration. The results in Fig. 6b help to separate out the effects of E_r and T_g on nanoindentation response. In particular, Fig. 6b indicates that the glass transition temperature is more significant than the rubbery modulus as a predictor of the materials response to nanoindentation in the glassy state. The drop in the glass transition temperature of the 25DEG25PEG50*t*BA (see Fig. 3c) results in considerable drop in hardness compared to the 50DEG50*t*BA even though these two materials have comparable crosslink density measured through rubbery modulus. Moreover, the hardness (vis-a-vis max and min penetration depths) of the 25DEG25PEG50*t*BA material is slightly lower than the 10DEG90*t*BA despite the higher crosslink density and rubbery modulus in the former material (both have a similar glass transition). This quantitative trend will be clearer in subsequent data analysis, although it is insightful to consider qualitative trends in the load–depth curves since these interpretations do not involve the assumptions inherent to quantitative analysis.

We have performed subsequent analysis on the load–depth curves shown in Fig. 6 to quantify various trends in indentation data, and provide statistical information. The analysis includes all data from duplicate experiments to quantify statistical variability. The indentation hardness, calculated from Eqs. (1)–(3), as a function of crosslink density is shown in Fig. 7a while the modulus as a function of crosslinker is shown in Fig. 7b. The error bars in Fig. 7a and b represent one standard deviation from the dataset mean. The inherent variations in both the hardness and modulus data can be partially driven by inhomogeneities in the material structure, due to material preparation. Previous work in Ref. [44] elucidates the effects of material preparation on the mechanical properties of polymers. The data in Table 1 shows that the maximum crosslink spacing is less than 2 nm. For a Berkovich tip of radius (150 nm) and the depth of penetration into the surface (1000 nm) the stress zone beneath the nanoindenter tip samples a statistically significant fraction of crosslinks at maximum load, a region that likely characterizes a representative volume element for this material. Aside from material and surface factors, measurement uncertainty can be derived from the incipient unloading part of the indentation curve [40,56]. One possible explanation for the uncertainty in the slope determination is the creep-viscoelastic properties inherent in polymers at the start of unloading. Similar patterns have been reported in the literature [57]. A trapezoidal loading–unloading curve was used to minimize this effect, as given in Ref. [43].

For experimental error, statistically significant trends exist in ambient temperature hardness, but not modulus, as a function of pure (DEGDMA) crosslinking. The elastic moduli extracted from nanoindentation are juxtaposed with measurements of modulus from tensile tests in Fig. 7b. While the ambient temperature nanoindentation modulus does not follow any statistically significant behavior with respect to increasing crosslink density, there is a slight trend of increasing modulus with increasing crosslink density in the tensile modulus data. Interestingly, the scatter in modulus data is significant for both the tensile and nanoindentation tests, although both techniques provide values that are in general agreement.

It is observed that as the crosslink density increases (crosslink spacing decreases), the hardness of the materials increases (Fig. 7a). This finding is due to the fact that for smaller crosslink spacing, the chains are restricted from conformational

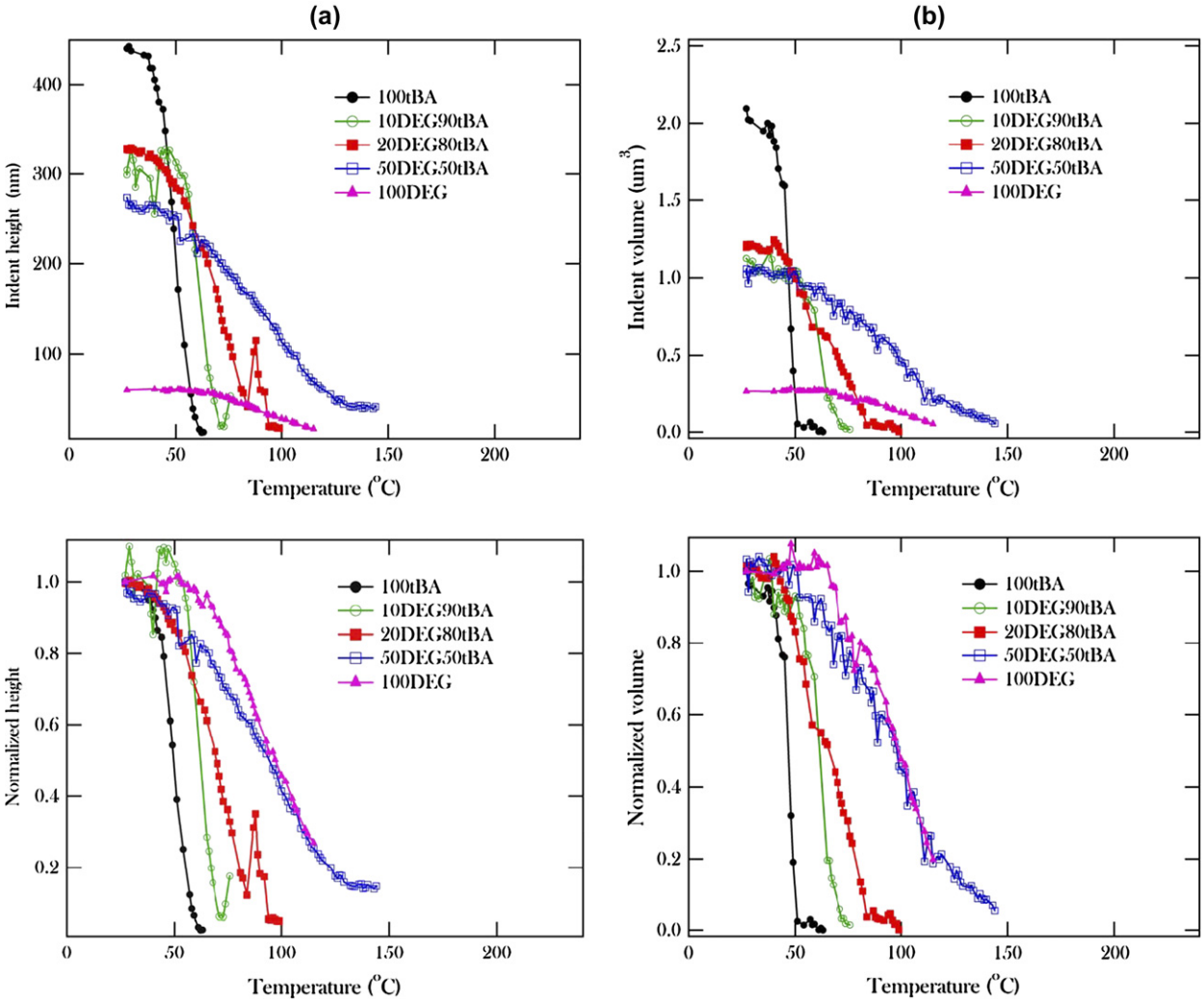

Fig. 9. (a) Evolution of indent peak-to-peak height with temperature for the DEGDMA-*co*-*t*BA materials. The figure at the bottom is the normalized peak-to-peak height with respect to the peak-to-peak height at room temperature. (b) Calculated indent volume based on indent height sweeps of DEGDMA-*co*-*t*BA materials. The figure at the bottom is the normalized peak-to-peak volume with respect to the peak-to-peak volume at room temperature.

motion due to the increasingly immobile network (a phenomenon that also increases T_g). To achieve large strain deformation required for a permanent impression below the glass transition temperature, the polymer chains must experience conformational motion, which is more difficult for higher crosslinked materials based on the measured increase in glass transition temperature. Consequently, the smallest crosslink spacing for 100DEG renders it the hardest of the materials in the present investigation, while the uncrosslinked material, 100*t*BA, is the softest.

From the DEGDMA data in Fig. 7a, it is clear that increasing crosslink density increases hardness, but it is unclear how to relate this increase to fundamental polymer properties since both glass transition and rubbery modulus of the DEGDMA networks increase with increasing crosslinker. Both rubbery modulus and glass transition temperature could potentially influence hardness data since both are linked to the ability of the materials to undergo conformation motion at a given temperature and stress, and both can be signatures of changes in crosslink density. Consistent with representative load–depth curves, the hardness of the 25DEG25PEG50*t*BA materials is significantly lower than the 50DEG50*t*BA and slightly lower than the 10DEG50*t*BA material (Fig. 7a). This important trend highlights the importance of T_g relative to the testing temperature, which is apparently more significant than the rubbery modulus in indentation response below glass transition. Consequently, the increase in hardness observed in Fig. 7a scales more with T_g with increasing DEGDMA rather than just crosslink density itself (measured via rubbery modulus). In fact, increasing crosslink density and rubbery modulus without influencing T_g has little effect on hardness (compare 10DEG50*t*BA and 25DEG25PEG50*t*BA which have similar T_g but much different rubbery modulus). This hypothesis is consistent with the flow behavior of glassy polymers below their glass transition temperature, where the slope of the hardening modulus during flow is more dependent on the vicinity to T_g rather than factors that control entropic elasticity and conformational stiffness [58].

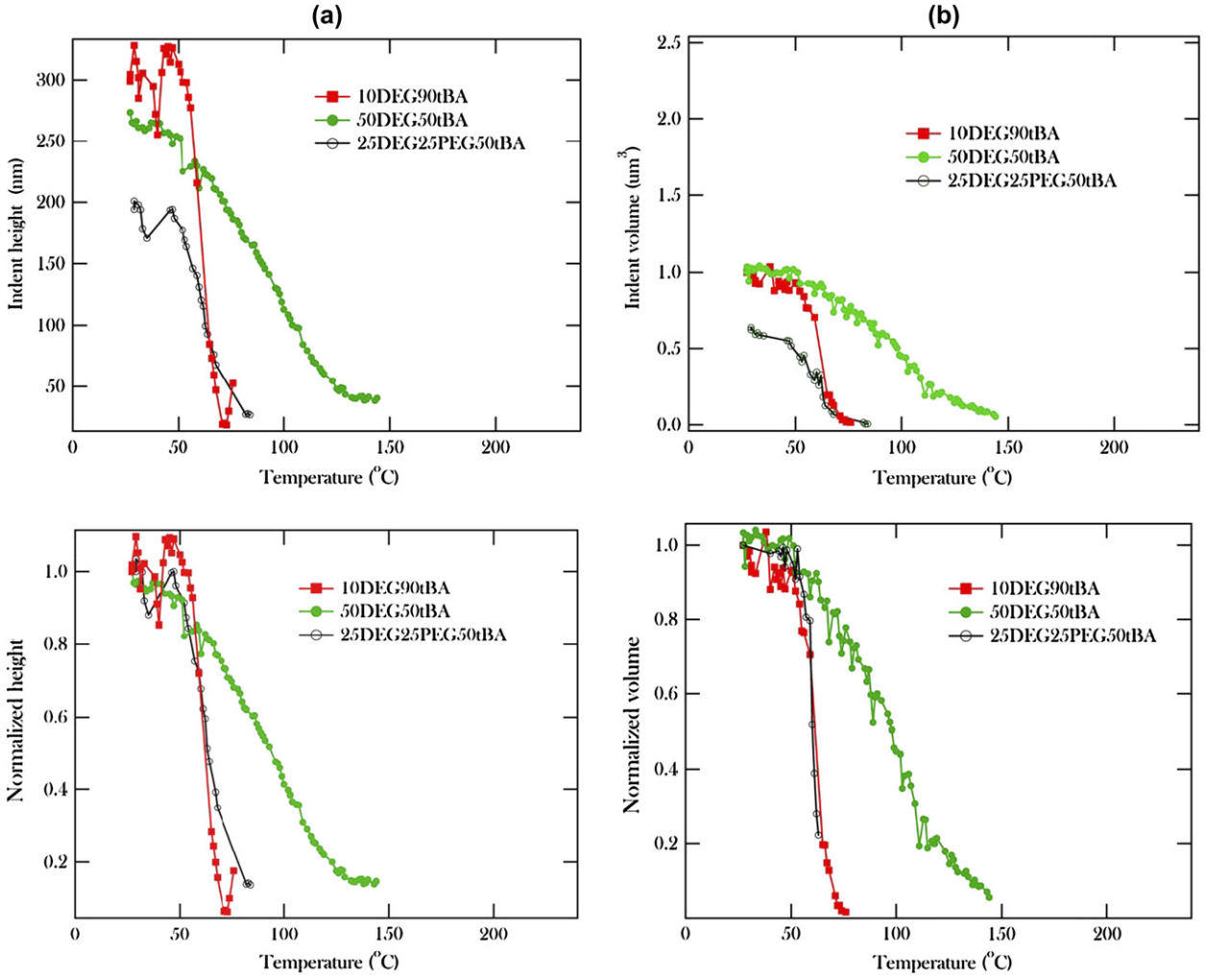

Fig. 10. (a) Evolution of indent peak-to-peak height with temperature for the 10DEG90*t*BA, 50DEG50*t*BA, and 25DEG25PEG50*t*BA. The figure at the bottom is the normalized peak-to-peak height with respect to the peak-to-peak height at room temperature. (b) Calculated indent volume based on indent height sweeps of 10DEG90*t*BA, 50DEG50*t*BA, and 25DEG25PEG50*t*BA. The figure at the bottom is the normalized peak-to-peak volume with respect to the peak-to-peak volume at room temperature.

The enclosed area between the loading and unloading curves is defined as the energy of dissipation [43,52], and is shown in Fig. 7c as a function of crosslinker fraction. Once again, the error bars are within one standard deviation of the mean. The energy dissipation is another tool that can be used to compare the different materials. Since the materials used in this study show elasto-plastic characteristics as depicted in Fig. 6a and b, it is expected that some energy will be dissipated as a result of the plastic deformation. It is evident from Fig. 7c that there is an inverse correlation between the dissipation energy and the wt% of crosslinking. As a result, the recoverable energy increases with increasing crosslinking. This finding may be explained in terms of the formidable opposition offered to conformational motions by the crosslinker molecules [59]. Of course, the energy dissipation is strongly dependent on the vicinity of the polymer to its glass transition temperature, where it shows maximum loss during cyclic loading and unloading. Consequently, the change in dissipation with increasing crosslinking can also be linked to the change in the glass transition temperature of the network.

The present results highlight the importance of considering differences in glass transition temperature relative to testing temperature when evaluating nanoindentation data. It is obvious that indentation response as a function of temperature will depend very strongly on the overall location of the testing temperature with respect to the glass transition (glassy, viscoelastic, versus rubbery). However, the results here indicate that below the glass transition temperature, hardness (not modulus) depends on vicinity of the glass transition temperature. This effect can cause a limitation when probing polymer structure or chemistry effects in polymers that have varying glass transition accompanying their structural changes or a glass transition temperature that varies with film thickness or near the material surface. Or, conversely, this effect may be useful for estimating changes in transition temperature in small volumes of material that cannot have transition temperatures measured using conventional methods.

Recovery of the indents created at ambient temperature was studied for a constant heating rate using atomic force microscopy. Representative tapping mode AFM topographical scans

of the indents are presented in Fig. 8 for 100*t*BA and 50DEG50*t*BA. Similar images were obtained for all materials. Fig. 9a displays the indent peak-to-peak height sweeps and normalized peak-to-peak heights with respect to the initial room temperature indent height. Fig. 9b presents the measured and normalized recovery volume as a function of temperature for the DEGDMA crosslinked material. The scans show recovery as the temperature is ramped. At temperatures in proximity to or in excess of T_g, the stored intermolecular forces between crosslinks act through an increase in free volume, allowing a reduction in stored entropy [52,60] culminating in the recovery of the deformed material. The recovery occurs at lower temperatures for materials with less crosslinking density and lower glass transition temperature, as expected based on results herein. Within measurement resolution, the materials recover all the imposed permanent deformation at a temperature in the vicinity of their T_g.

A similar recovery pattern is observed in Fig. 10a and b, for the 10DEG90*t*BA, 50DEG50*t*BA, and 25DEG25PEG50*t*BA materials. Here, higher temperatures are required to recover the impressions in the 50DEG50*t*BA material relative to the other two due to its higher glass transition temperature. The similarity between the recovery profile of the 10DEG90*t*BA and the 25DEG25PEG50*t*BA indicate that the rubbery modulus is not strongly influencing the free strain recovery, even though the higher rubbery modulus does provide additional entropic driving force during recovery. The additional entropic driving force present during free recovery is apparently not significant enough to alter free strain recovery profile in light of the large effect of temperature on free volume, which enables the entropic effect to act. However, it should be noted that the 25DEG25PEG50*t*BA material with higher crosslink density and rubbery modulus should provide larger force during constrained recovery, although this effect was not explored here.

5. Conclusion

We have investigated the dependence of the bulk and nanomechanical properties of shape memory polymer networks on crosslink density. This research provides a foundation to understand and further explore the nanomechanical behavior of shape memory polymers. The following primary conclusions have been drawn:

1. The ambient temperature modulus showed a slight, but statistically insignificant dependence on the crosslinker concentration measured using both nanoindentation and tensile testing.
2. The ambient temperature hardness showed a statistically significant increase as a function of crosslinker concentration. Using a designed material, the increase was shown to correlate to glass transition temperature rather than rubbery modulus.
3. All indents showed recovery during heating above their glass transition temperature. Free strain recovery temperature was strongly influenced by crosslinker concentration through changes in glass transition temperature but not rubbery modulus.

References

[1] Shmulewitz A, Langer R, Patton J. Nature Biotechnology 2006;24(3):277–80.
[2] Yu Q, Zhang JZ, Cheng ML, Zhu SP. Macromolecular Chemistry and Physics 2006;207(3):287–94.
[3] Small W, Metzger MF, Wilson TS, Maitland DJ. IEEE Journal of Selected Topics in Quantum Electronics 2005;11(4):892–901.
[4] Haller I, Stewart KJ. Journal of Vacuum Science and Technology B: Microelectronics Processing and Phenomena (USA) 1991;3370–3. Seattle, WA, USA.
[5] Rauter H, Matyushin V, Alguel Y, Pittner F, Schalkhammer T. Macromolecular Symposia 2004;217:109–33.
[6] Yang ZH, Hu JL, Liu YQ, Yeung LY. Materials Chemistry and Physics 2006;98(2–3):368–72.
[7] Collie GJ, Black I. Proceedings of the Institution of Mechanical Engineers Part E – Journal of Process Mechanical Engineering 2005;219(4):345–55.
[8] Feger C. Proceedings of fourth international symposium on advanced packaging materials processes, properties and interfaces (Cat. no. 98EX153). Braselton, GA, USA: IEEE; 1998. p. 77–81.
[9] Speidell JL, Pulaski DP, Patel RS. IBM Journal of Research and Development 1997;41(1–2):143–9.
[10] Shih DY, Lewis J, Yeh H, Graham W, Paraszczak J, Nunes S, et al. ISHM '92 proceedings. Proceedings of the 1992 international symposium on microelectronics (SPIE Vol. 1847). San Francisco, CA, USA: Int. Soc. Hybrid Microelectron; 1992. p. 376–83.
[11] Umbach CP, Broers AN, Willson CG, Koch R, Laibowitz RB. Journal of Vacuum Science and Technology B: Microelectronics Processing and Phenomena (USA) 1988;319–22. Woodland Hills, CA, USA.
[12] Hatzakis M, Shaw J, Babich E, Paraszczak J. Journal of Vacuum Science and Technology B: Microelectronics Processing and Phenomena (USA) 1988;2224–8. Fort Lauderdale, FL, USA.
[13] Babich E, Shaw J, Hatzakis M, Paraszczak J, Witman D, Grenon BJ. Microelectronic Engineering (Netherlands) 1986;299–313. Interlaken, Switzerland.
[14] Saarela V, Franssila S, Tuomikoski S, Marttila S, Ostman P, Sikanen T, et al. Sensors and Actuators B: Chemical 2006;114(1):552–7.
[15] Knoll A, Bachtold P, Bonan J, Cherubini G, Despont M, Drechsler U, et al. Microelectronic Engineering 2006;83(4–9):1692–7.
[16] Gall K, Yakacki CM, Liu YP, Shandas R, Willett N, Anseth KS. Journal of Biomedical Materials Research Part A 2005;73(3):339–48.
[17] Sipahigil O, Torres-Lugo M, Peppas NA. STP Pharma Sciences 2002;12(6):345–50.
[18] Kallrot M, Edlund U, Albertsson AC. Biomaterials 2006;27(9):1788–96.
[19] Feng W, Brash JL, Zhu S. Biomaterials 2006;27(6):847–55.
[20] Frost RL, Mendelovici E. Journal of Colloid and Interface Science 2006;294(1):47–52.
[21] Harbers GM, Healy KE. Journal of Biomedical Materials Research Part A 2005;75(4):855–69.
[22] Mathieu LM, Mueller TL, Bourban P-E, Pioletti DP, Muller R, Manson J-AE. Biomaterials 2006;27(6):905–16.
[23] Nagesh K, Ramakrishnan S. Synthetic Metals 2005;155(2):320–3.
[24] Reddy SK, Sebra RP, Anseth KS, Bowman CN. Journal of Polymer Science Part A: Polymer Chemistry 2005;43(10):2134–44.
[25] Ward JH, Shahar A, Peppas NA. Polymer 2002;43(6):1745–52.
[26] Lendlein A, Jiang HY, Junger O, Langer R. Nature 2005;434(7035):879–82.
[27] Mohr R, Kratz K, Weigel T, Lucka-Gabor M, Moneke M, Lendlein A. Proceedings of the National Academy of Sciences 2006;103(10):3540–5.
[28] Huang WM, Lee CW, Teo HP. Journal of Intelligent Material Systems and Structures 2006;17(8–9):753–60.
[29] Schmidt AM. Macromolecular Rapid Communications 2006;27(14):1168–72.

[30] Liu G, Guan C, Xia H, Guo F, Ding X, Peng Y. Macromolecular Rapid Communications 2006;27(14):1100–4.
[31] Gall K, Kreiner P, Turner D, Hulse M. Journal of Microelectromechanical Systems 2004;13(3):472–83.
[32] Liu YP, Gall K, Dunn ML, McCluskey P. Mechanics of Materials 2004;36(10):929–40.
[33] Wei ZG, Sandstrom R, Miyazaki S. Journal of Materials Science 1998;33(15):3743–62.
[34] Wei ZG, Sandstrom R, Miyazaki S. Journal of Materials Science 1998; 33(15):3763–83.
[35] Duncheon C. Industrial Robot: An International Journal 2005;32(6): 452–5.
[36] Loubet JL, Georges JM, Marchesini O, Meille G. Journal of Tribology-Transactions of the ASME 1984;106(1):43–8.
[37] Jiang S, Li X, Guo S, Hu Y, Yang J, Jiang Q. Smart Materials and Structures 2005;14(4):769–74.
[38] Shaw GA, Trethewey JS, Johnson AD, Drugan WJ, Crone WC. Advanced Materials 2005;17(9):1123–7.
[39] Yuan ZY, Xu D, Ye ZC, Cai BC. Journal of Materials Science and Technology 2005;21(3):319–23.
[40] VanLandingham MR, Villarrubia JS, Guthrie WF, Meyers GF. Macromolecular Symposia 2001;167:15–43.
[41] Briscoe BJ, Fiori L, Pelillo E. Journal of Physics D: Applied Physics 1998;31(19):2395–405.
[42] Shen L, Phang IY, Liu TX, Zeng KY. Polymer 2004;45(24):8221–9.
[43] Klapperich C, Komvopoulos K, Pruitt L. Journal of Tribology-Transactions of the ASME 2001;123(3):624–31.
[44] Wright-Charlesworth DD, Miller DM, Miskioglu I, King JA. Journal of Biomedical Materials Research Part A 2005;74(3):388–96.
[45] Gregory JR, Spearing SM. Composites Science and Technology 2005; 65(3–4):595–607.
[46] Xu WH, Xiao ZY, Zhang TY. Materials Letters 2005;59(17):2153–5.
[47] Yu SZ, Wong TKS, Hu X, Wei J, Yong MS. Microelectronic Engineering 2005;77(2):125–31.
[48] Tweedie CA, Van Vliet KJ. Journal of Materials Research 2006;21(6): 1576–89.
[49] Lee BS, Chun BC, Chung YC, Sul KI, Cho JW. Macromolecules 2001;34(18):6431–7.
[50] Tobushi, Hayashi, Hoshio, Miwa. Smart Materials and Structures 2006;15(4):1033–8.
[51] Lim G, Park K, Sugihara M, Minami K, Esashi M. Sensors and Actuators A: Physical 1996;56(1–2):113–21.
[52] Nelson BA, King WP, Gall K. Applied Physics Letters 2005;86(10).
[53] Oliver WC, Pharr GM. Journal of Materials Research 1992;7(6):1564–83.
[54] Elliott JE, Bowman CN. Polymer Reaction Engineering 2002;10(1–2): 1–19.
[55] Schwaller P, Haug FJ, Michler J, Patscheider J. Advanced Engineering Materials 2005;7(5):318–22.
[56] Malzbender J, den Toonder JMJ, Balkenende AR, de With G. Materials Science and Engineering R: Reports 2002;36(2–3):47–103.
[57] Vanlandingham MR, McKnight SH, Palmese GR, Elings JR, Huang X, Bogetti TA, et al. Journal of Adhesion 1997;64(1–4):31–59.
[58] van Melick HGH, Govaert LE, Meijer HEH. Polymer 2003;44(8): 2493–502.
[59] Andreas Lendlein SK. Angewandte Chemie International Edition 2002;41(12):2034–57.
[60] Tobushi H, Matsui R, Hayashi S, Shimada D. Smart Materials and Structures 2004;13(4):881–7.